AFRL-VA-WP-TP-2006-331

AN AEROTHERMAL FLEXIBLE MODE ANALYSIS OF A HYPERSONIC VEHICLE (POSTPRINT)

Trevor Williams, Michael A. Bolender, David B. Doman, and Oscar Morataya

JULY 2006

Approved for public release; distribution is unlimited.

STINFO COPY

AIR VEHICLES DIRECTORATE
AIR FORCE MATERIEL COMMAND
AIR FORCE RESEARCH LABORATORY
WRIGHT-PATTERSON AIR FORCE BASE, OH 45433-7542

NOTICE AND SIGNATURE PAGE

Using Government drawings, specifications, or other data included in this document for any purpose other than Government procurement does not in any way obligate the U.S. Government. The fact that the Government formulated or supplied the drawings, specifications, or other data does not license the holder or any other person or corporation; or convey any rights or permission to manufacture, use, or sell any patented invention that may relate to them.

This report was cleared for public release by the Air Force Research Laboratory Wright Site (AFRL/WS) Public Affairs Office and is available to the general public, including foreign nationals. Copies may be obtained from the Defense Technical Information Center (DTIC) (http://www.dtic.mil).

AFRL-VA-WP-TP-2006-331 HAS BEEN REVIEWED AND IS APPROVED FOR PUBLICATION IN ACCORDANCE WITH ASSIGNED DISTRIBUTION STATEMENT.

*//Signature//

Michael A. Bolender
Aerospace Engineer
Control Design and Analysis Branch
Air Force Research Laboratory
Air Vehicles Directorate

//Signature//

Deborah S. Grismer
Chief
Control Design and Analysis Branch
Air Force Research Laboratory
Air Vehicles Directorate

//Signature//

JEFFREY C. TROMP
Senior Technical Advisor
Control Sciences Division
Air Vehicles Directorate

This report is published in the interest of scientific and technical information exchange, and its publication does not constitute the Government's approval or disapproval of its ideas or findings.

*Disseminated copies will show "//Signature//" stamped or typed above the signature blocks.

REPORT DOCUMENTATION PAGE

Form Approved
OMB No. 0704-0188

1. REPORT DATE *(DD-MM-YY)*	2. REPORT TYPE	3. DATES COVERED *(From - To)*
July 2006	Conference Paper Postprint	06/15/2006– 07/28/2006

4. TITLE AND SUBTITLE

AN AEROTHERMAL FLEXIBLE MODE ANALYSIS OF A HYPERSONIC VEHICLE (POSTPRINT)

5a. CONTRACT NUMBER
In-house

5b. GRANT NUMBER

5c. PROGRAM ELEMENT NUMBER
N/A

6. AUTHOR(S)

Trevor Williams and Oscar Morataya (University of Cincinnati)
Michael A. Bolender and David B. Doman (AFRL/VACA)

5d. PROJECT NUMBER
A03D

5e. TASK NUMBER

5f. WORK UNIT NUMBER
0B

7. PERFORMING ORGANIZATION NAME(S) AND ADDRESS(ES)

University of Cincinnati
Dept. of Aerospace Engineering
Cincinnati, OH 45221-0070

Control Design and Analysis Branch (AFRL/VACA)
Control Sciences Division
Air Vehicles Directorate
Air Force Materiel Command, Air Force Research Laboratory
Wright-Patterson Air Force Base, OH 45433-7542

8. PERFORMING ORGANIZATION REPORT NUMBER
AFRL-VA-WP-TP-2006-331

9. SPONSORING/MONITORING AGENCY NAME(S) AND ADDRESS(ES)

Air Vehicles Directorate
Air Force Research Laboratory
Air Force Materiel Command
Wright-Patterson Air Force Base, OH 45433-7542

10. SPONSORING/MONITORING AGENCY ACRONYM(S)
AFRL-VA-WP

11. SPONSORING/MONITORING AGENCY REPORT NUMBER(S)
AFRL-VA-WP-TP-2006-331

12. DISTRIBUTION/AVAILABILITY STATEMENT
Approved for public release; distribution is unlimited.

13. SUPPLEMENTARY NOTES

This work was published in the Proceedings of the AIAA Atmospheric Flight Mechanics Conference and Exhibit.

PAO Case Number: AFRL/WS 06-1934 (cleared August 9, 2006).

14. ABSTRACT

This paper describes a method for the determination of the flexible modes of an air-breathing hypersonic vehicle. The method outlined here takes into account changes in vehicle mass and structural temperature over the duration of the vehicle's trajectory. A simple sizing program is outlined to estimate the vehicle volume, mass, and planform requirements for a dual-cycle (rocket and scramjet) powered vehicle. It is shown that the varying mass effects dominate the frequencies and mode-shapes over the structural heating effects. We then discuss the effects of the structural modes on the transmission zeros.

15. SUBJECT TERMS

16. SECURITY CLASSIFICATION OF:			17. LIMITATION OF ABSTRACT:	18. NUMBER OF PAGES	19a. NAME OF RESPONSIBLE PERSON (Monitor)
a. REPORT	b. ABSTRACT	c. THIS PAGE			Michael Bolender
Unclassified	Unclassified	Unclassified	SAR	28	19b. TELEPHONE NUMBER *(Include Area Code)* N/A

Standard Form 298 (Rev. 8-98)
Prescribed by ANSI Std. Z39-18

An Aerothermal Flexible Mode Analysis of a Hypersonic Vehicle

Trevor Williams *
Department of Aerospace Engineering
University of Cincinnati
Cincinnati, OH 45221-0070

Michael A. Bolender †
David B. Doman ‡
Air Force Research Laboratory
Wright-Patterson AFB, OH 45433

Oscar Morataya §
Department of Aerospace Engineering
University of Cincinnati
Cincinnati, OH 45221-0070

This paper describes a method for the determination of the flexible modes of an air-breathing hypersonic vehicle. The method outlined here takes into account changes in vehicle mass and structural temperature over the duration of the vehicle's trajectory. A simple sizing program is outlined to estimate the vehicle volume, mass, and planform requirements for a dual-cycle (rocket and scramjet) powered vehicle. It is shown that the varying mass effects dominate the frequencies and mode-shapes over the structural heating effects. We then discuss the effects of the structural modes on the transmission zeros.

I. Introduction

The renewed interest in hypersonic vehicles (HSVs) stems from the U.S. Air Force's desire to achieve two objectives. The first is reliable and affordable access to space. The second is

*Professor. Associate Fellow AIAA
†Aerospace Engineer. Senior Member AIAA.
‡Senior Aerospace Engineer. Associate Fellow AIAA.
§Graduate Student. Student Member AIAA

to respond quickly to serious threats around the globe. In each case, air-breathing hypersonic vehicle concepts are being explored to achieve these goals. To enable affordable space access, an HSV would likely comprise the second stage of a two-stage-to-orbit vehicle. The second stage would accelerate from Mach 4 to Mach 15 using a scramjet. Beginning at Mach 15, the remainder of the ascent would then occur under the power of a rocket engine to achieve orbit. To achieve a prompt global strike capability, it is envisioned that a hypersonic cruise vehicle would be launched from the continental United States to deliver conventional weapons to a target anywhere in the world. Such an aircraft would possibly use either a turbine-based or a rocket-based combined-cycle engine to accelerate to hypersonic speeds, at which point the scramjet would take over for the remainder of the climb and cruise segments of the mission.

From the point-of-view of the flight controls engineer, there is little difference between the two concepts as they each offer the same set of technological challenges with regards to inner-loop and outer-loop control. Scramjet powered vehicles require an integrated airframe/propulsion system in order to optimize system performance. The level of integration of the scramjet results in a system whose engine dynamics and performance are dependent upon the aircraft's angle-of-attack, Mach number, and altitude. The engine also has a significant influence on the lift, drag, and pitching moment of the aircraft. Also, the structural dynamics can have a significant effect on the engine performance. Deflection of the aircraft's forebody due to aerodynamic forces will change the apparent turn angle-of-the flow, thus altering the pressure distribution along the forebody and perturbing the mass flow of air through the engine. Capturing the effect of the structural dynamics are vital to designing a robust control system. A controls based model has been developed by Bolender and Doman[1] to study vehicle configurations early in the design cycle in order to identify any issues that could affect the controllability of the vehicle and to optimize inner and outer-loop performance. For this paper, we will focus on a cruise vehicle configuration (see Figure 1); however, the results are general enough that they apply to an accelerator as well.

This paper describes a flexible mode analysis of an HSV that takes into account the decrease in propellant mass over the course of its mission. As a first step, it is necessary to size a vehicle that is capable of performing the specified mission. We outline a method that initially sizes the vehicle to estimate the required structural and fuel masses given the payload and cruise range requirements for a cruise-type HSV. An operational cruise HSV would be expected to be designed to operate over a long range at high speed. This dictates that a large fraction of the gross take-off weight of the vehicle must consist of propellant for both the climb and cruise phases of the mission (it is assumed that the fuel requirements during descent are insignificant). The mass properties of the vehicle will therefore change considerably as the mission progresses and propellant is consumed. This will in turn cause significant changes in the structural modes of the HSV.

The objective of the subsequent analysis is to determine the evolution of the natural frequencies, as well as of the associated mode shapes. The approach taken here is the *assumed modes method*,[2] a technique that makes use of the mode shapes of a simple structure (e.g., a cantilever beam) as a set of basis functions that are then used to generate a set of approximate mode shapes for the actual structure, and accounts for the actual mass and stiffness distribution of the true structure. Typically, as the number of basis functions in the model is increased, convergence of the first approximate natural frequencies and mode shapes to the true frequencies improves rapidly. The assumed modes method not only allows the effects of propellant depletion on the HSV natural frequencies and mode shapes to be

quantified; it also allows one to study the effects of temperature on vehicle stiffness and the associated changes in the modal characteristics.

Figure 1. X-43C Concept Vehicle

II. Trajectory Analysis and Vehicle Sizing

The design of hypersonic aircraft offers a unique set of challenges because they operate over such a wide range of flight conditions. The primary challenge, however, lies in the design of the propulsion system. Supersonic combustion ramjet (scramjet) propulsion is the most studied approach for hypersonic speed domain, but it is only becomes practical when the Mach number becomes greater than 5. The concepts for getting the aircraft airborne and accelerated to the speed where the scramjet can be operated are seemingly endless. For example, if we consider a two-stage-to-orbit (TSTO) vehicle, the HSV comprises the upper stage of the launch system. The vehicle is boosted by a rocket-powered first stage to some staging Mach number. The vehicles separate and the second stage continues its ascent while being powered by a scramjet engine. At some point a rocket engine takes over again, and continues to boost the vehicle to low-earth orbit. For cruise vehicles, combined-cycle engines, either rocket-based or turbine-based, have been investigated as a means for propulsion. Some of the concepts are single-flow path with an engine that can operate using different cycles. Other concepts require multiple flowpaths and/or engines. The interested reader is referred to Czysz, et.al.[3] for a discussion of different propulsion system concepts and one approach to the sizing of hypersonic aircraft.

Below, we approach the sizing of the vehicle in terms of the range and payload requirement. A simplified analysis is presented in Gregory, et.al.[4] that assumes that the Breguet

Range Equation can be applied over the entire trajectory using averaged values for specific impulse, L/D, and velocity. This assumes that a majority of the flight is at the cruise condition. While this is indeed the case for long trajectories, a slightly more rigorous approach can allow one to evaluate how the trajectory design interacts with propulsion system and aerodynamic efficiencies. However, our motivation is to estimate the fuel requirements along the entire trajectory in order to estimate the mass properties of the vehicle at any flight condition. For our purposes, it is assumed that the scramjet-powered ascent trajectory consists of climbs at either constant dynamic pressure or constant Mach number and that the cruise condition is at the same Mach number as the constant Mach climb segment. The rocket-powered phase will be treated separately using the rocket equation and assumed losses in ΔV in order to estimate the weight ratio.

A. Constant Dynamic Pressure Climb

We begin with the point-mass equations-of-motion for a vehicle flying over a flat earth. It is assumed throughout this analysis that the thrust vector is aligned with velocity vector. We will not consider the centripetal relief due to the high velocity and the altitude at which the vehicle is flying. The "flat earth" assumption will give conservative estimates for range later on.

$$\dot{V} = \left(\frac{F_n - D}{W} - \sin\gamma\right) g \tag{1}$$

$$\dot{\gamma} = \left(\frac{L}{W} - \cos\gamma\right) \frac{g}{V} \tag{2}$$

$$\dot{h} = V \sin\gamma \tag{3}$$

$$\dot{x} = V \cos\gamma \tag{4}$$

$$\dot{W} = -c_T F_n \tag{5}$$

where V is the airspeed, F_n is the thrust, D is the drag, W is the weight, γ is the flight-path angle (measured with respect to the horizon), g is the acceleration due to gravity, L is the lift, x is the downrange, and c_T is the thrust-specific fuel consumption and has units of $\mathrm{lb_m/sec/lb_f}$ or 1/sec. The dynamic pressure is given by

$$\bar{q} = \frac{1}{2}\rho_\infty V^2 \tag{6}$$

where ρ_∞ is the freestream air density.

Imposing the constraint that $\bar{q}$ is a constant specifies the velocity profile since the density as a function of altitude is known. Differentiating $\bar{q}$ with respect to altitude we have

$$\frac{d\bar{q}}{dh} = \frac{V^2}{2}\frac{d\rho}{dh} + \rho V \frac{dV}{dh} = 0 \tag{7}$$

Solving for dV/dh gives

$$\frac{dV}{dh} = -\frac{V}{2}\frac{1}{\rho}\frac{d\rho}{dh} \tag{8}$$

If we assume that the density profile is an exponential function of altitude

$$\rho = \rho_0 \exp\left(-\frac{h - h_0}{h_s}\right) \tag{9}$$

where ρ_0 is the density at some reference altitude h_0 and $h_s = RT_0/g$ is the scale height where T_0 is the ambient temperature at the altitude h_0. It can then be shown that

$$\frac{1}{\rho}\frac{d\rho}{dh} = -\frac{1}{h_s} \tag{10}$$

Over the length of the trajectory, it is assumed that $\dot{\gamma} \approx 0$ such that $L/W = \cos\gamma$. Next, we apply The Chain Rule to Equations 1 and 5. Beginning with Equation 1 we have:

$$V \sin\gamma \frac{dV}{dh} = \left(\frac{F_n - D}{W} - \sin\gamma\right) g \tag{11}$$

Collecting like terms and substituting $W = L/\cos\gamma$ gives

$$\left(1 + \frac{V}{g}\frac{dV}{dh}\right)\sin\gamma = \frac{F_n}{W} - \frac{D}{L}\cos\gamma \tag{12}$$

Solving for F_n/W gives

$$\frac{F_n}{W} = \left(1 + \frac{V}{g}\frac{dV}{dh}\right)\sin\gamma + \frac{D}{L}\cos\gamma \tag{13}$$

Applying The Chain Rule to Equation 5 gives

$$\frac{1}{W}\frac{dW}{dh} = -\frac{c_T}{V\sin\gamma}\frac{F_n}{W} \tag{14}$$

Next, we substitute Equations 13, 8 and 10 into Equation 14 to give:

$$\frac{1}{W}\frac{dW}{dh} = -c_T\left[\frac{D}{L}\frac{\cot\gamma}{V} + \left(1 + \frac{V^2}{2gh_s}\right)\frac{1}{V}\right] \tag{15}$$

Note that to integrate Equation 15 requires the velocity profile be given. From the dynamic pressure, we know that the velocity is

$$V = \sqrt{\frac{2\bar{q}}{\rho}} \tag{16}$$

Substituting for the density then gives

$$V = \sqrt{\frac{2\bar{q}}{\rho_0}}\exp\left(\frac{h - h_0}{2h_s}\right) \tag{17}$$

Equation 17 can be simplified further if we define $V_0 = \sqrt{2\bar{q}/\rho_0}$, giving

$$V = V_0 \exp\left(\frac{h - h_0}{2h_s}\right) \tag{18}$$

Using Equation 18 and assuming that c_T, L/D and γ are constant over the climb allows us to integrate the Equation 15 analytically from an altitude of h_1 to an altitude of h_2, giving us

$$\ln\left(\frac{W_2}{W_1}\right) = h_s c_T \left(\frac{D}{L}\cot\gamma + 1\right)\left(\frac{1}{V(h_2)} - \frac{1}{V(h_1)}\right) + \frac{c_T}{2g}\Big(V(h_2) - V(h_1)\Big) \tag{19}$$

More accurate results can be obtained by letting c_T, the lift, and the drag vary over the trajectory segment while maintaining a constant flight path angle. In any case, the range covered in this segment of the climb is easily calculated by integrating Equation 4, yielding

$$\int_{h_1}^{h_2} \cot\gamma \, dh = (h_2 - h_1)\cot\gamma \tag{20}$$

B. Constant Mach Climb

The procedure for computing the weight change in a constant Mach climb is similar to that outlined above for a constant $\bar{q}$ climb. The difference is that we impose the constraint that Mach is a constant over some defined altitude range. The Mach number of the aircraft is defined as

$$M = \frac{V}{a} \tag{21}$$

where the speed-of-sound is given by $a = \sqrt{kRT}$, $k = 7/5$ is ratio of specific heats, and $R = 1716$ ft^2 s^2/°R is the gas constant for air. Differentiating Mach number with respect to altitude gives

$$\frac{dM}{dh} = 0 = \frac{1}{a}\frac{dV}{dh} - \frac{V}{a^2}\frac{da}{dh} \tag{22}$$

Solving for dV/dh gives

$$\frac{dV}{dh} = M\frac{da}{dh} \tag{23}$$

The differential equation for the fuel flow as a function of altitude is found by substituting Equations 13 and 23

$$\frac{1}{W}\frac{dW}{dh} = -\frac{c_T}{V}\left[\frac{D}{L}\cot\gamma + 1 + \frac{V}{g}\frac{dV}{dh}\right] \tag{24}$$

Multiplying the right-hand side of Equation 24 by a/a and simplifying gives:

$$\frac{1}{W}\frac{dW}{dh} = -\frac{c_T}{M}\left[\frac{D}{L}\frac{1}{a}\cot\gamma + \frac{1}{a} + \frac{M^2}{g}\frac{dV}{dh}\right] \tag{25}$$

To integrate Equation 25, we consider the following two cases: an isothermal layer of the atmosphere and a linear temperature lapse rate. We will once again assume that c_T, L/D and γ are constant.

1. *Case 1: $da/dh = 0$*

Substituting $da/dh = 0$ and integrating gives us

$$\ln\frac{W_2}{W_1} = -\frac{c_T}{M}\left(\frac{\cot\gamma}{a}\frac{D}{L} + \frac{1}{a}\right)\Big(h_2 - h_1\Big) \tag{26}$$

2. Case 2: $T = T_0 + \lambda(h - h_0)$

For the case where the temperature varies linearly with altitude, it can be shown that the speed-of-sound becomes

$$a = \sqrt{kR[T_0 + \lambda(h - h_0)]} \tag{27}$$

Thus, when we differentiate with respect to altitude we get

$$\frac{da}{dh} = \frac{\lambda kR}{2a} \tag{28}$$

Substituting and evaluating the integral gives us:

$$\ln \frac{W_2}{W_1} = -\frac{c_T}{M}\left[\frac{\cot\gamma}{L/D} + 1 + \frac{M^2}{2g}kR\lambda\right]\frac{2}{kR\lambda}\Big(a(h_2) - a(h_1)\Big) \tag{29}$$

C. Level Cruise

For flight over a flat earth, the Breguet Range Equation is

$$\ln \frac{W_2}{W_1} = -\frac{c_T}{V}\frac{D}{L}x \tag{30}$$

The range is the desired range minus the range covered in the climb to altitude: $x = x_{des} - x_{climb}$.

D. Rocket Powered Accelerating Climb

We consider the case where the rocket-powered vehicle climbs while accelerating from rest to the desired dynamic pressure. We will consider the vehicle to be capable of horizontal take-off; however, we neglect the ground roll and corresponding acceleration to the lift-off speed from rest since this comprises a very small part of the overall trajectory. As a first approximation, we will have the vehicle begin its climb from rest, but at some constant flight-path angle. The drag will be accounted for by adding a 10% ΔV to the final desired velocity, which is the Mach 5 point on some constant dynamic pressure climb profile. The Mach 5 point is chosen because this is considered the lowest Mach number at which supersonic combustion is feasible. To get the weight ratio for this segment of the flight, we simply use The Rocket Equation:

$$\frac{W_2}{W_1} = \exp\left(-\frac{\Delta V}{I_{sp}g}\right) \tag{31}$$

E. Determination of the Fuel Fraction

To determine the fuel fraction, we require the weight ratios on each segment of the trajectory. The overall ratio of the final weight to the initial weight at take-off is then

$$\frac{W_f}{W_0} = \frac{W_1}{W_0}\frac{W_2}{W_1}\cdots\frac{W_n}{W_{n-1}} \tag{32}$$

where n is the number of trajectory segments, W_0 is the gross take-off weight, and W_f=W_n is the weight at the end of the final segment.

F. Vehicle Sizing

For our analysis, we will focus on a rocket-based combined-cycle engine. The vehicle will be propelled by a rocket engine from take-off to Mach 5 and a dynamic pressure of 2000 psf. At this point, the scramjet engine begins operation and continues a climb while holding the dynamic pressure at 2000 psf. Once the aircraft reaches Mach 10, the aircraft holds this Mach number constant until it reaches its cruise altitude. The aircraft then cruises at Mach 10 at 120,000 ft for the duration of the mission. The range requirement is assumed to be 8000 n.m. while carrying a 2,500 lb payload. It is assumed the I_{sp} of the rocket-mode of the combined cycle-engine is 375 lb_f s/lb_m, the lift-to-drag ratio $L/D = 4.5$, and the thrust-specific fuel consumption of the scramjet is $c_T = 5.04 \times 10^{-4} \text{lb}_m/(\text{lb}_f\,\text{s})$, which corresponds to a scramjet $I_{sp} = 1985$ lb_f s/lb_m.

From above, we have $W_1/W_0 = 0.6432$ at the end of the rocket-powered phase, $W_2/W_1 = 0.7745$ at the end of the constant dynamic pressure climb, $W_3/W_2 = 0.9762$ at the end of the constant Mach climb. These three phases cover approximately 1125 n.mi., so our cruise range will be approximately 6875 n.mi. The weight fraction of fuel burned at the end of the cruise is then found using the Breguet Range Equation (Equation 30) is $W_f/W_3 = 0.6323$ This gives a ratio of final weight to take-off weight of $W_f/W_0 = 0.3071$. Thus, approximately 70% of the weight that the aircraft is lifting is attributed to fuel and oxidizer.

Sizing for the vehicle was done in a rather *ad hoc* manner in order to achieve a vehicle layout that would be qualitatively reasonable. The purpose being to have a representative vehicle to demonstrate the utility of the assumed modes approach for structural analysis. The sizing was done using the relationships outlined in Czysz's text.[5] This particular approach relies on empirical data to obtain relationships between volume, planform area, weight, etc.

Once the weight fraction above was obtained, we chose a value of Küchemann's "Tau":$\tau = V_{TOT}/(S_{plan})^{3/2} = 0.1$. For an assumed planform area, the Operational Weight Empty is approximated by $OWE = 61.6(S_{plan})^{0.906}$. We chose a planform area of 5500 ft^2, which gives OWE=151,000 lb. From above, the gross take-off weight is approximately 500,000 lb. The total volume is then 40,800 ft^3.

G. Internal Volume Layout

A preliminary vehicle layout was performed to get an estimate of how the vehicle total mass and the mass distribution changes as the fuel is used. Because the propulsion system is assumed to be a "dual-mode" engine that is capable of operating as either a rocket or a scramjet, an oxidizer tank is necessary for operation in the rocket mode. The fuel is assumed to be LH_2 and is contained in two tanks, one fore and one aft, that are assumed to be drained in a manner to keep the movement in the center-of-mass location to a minimum. The oxidizer, LO_2, is in a centrally mounted tank. This placement was chosen in order to keep the center-of-mass at a point that is in the neighborhood of 55% of the total vehicle length. Subsystems were placed in the most forward and aft locations possible, while the payload was assumed to be at the vehicle center-of-mass. A notional layout of the vehicle internal volume is given in Figure 2.

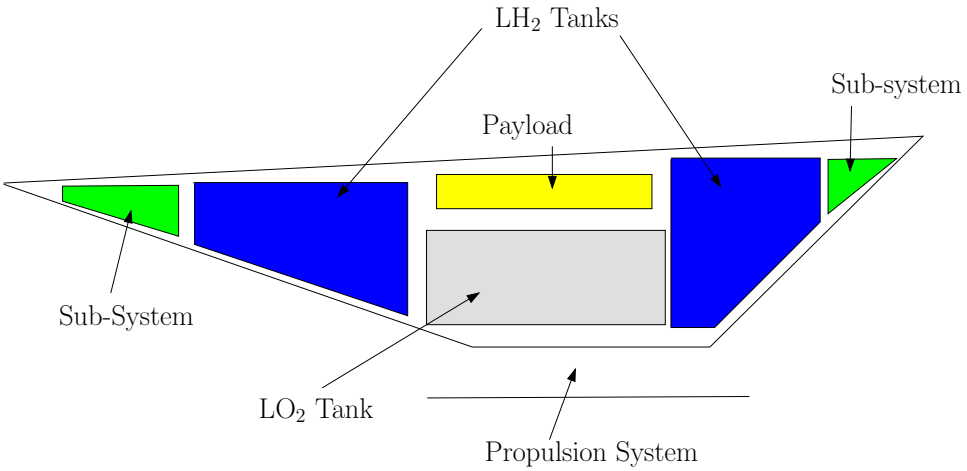

Figure 2. Notional Internal Volume Layout

III. Assumed Modes Method

The assumed modes method is a technique for computing the natural frequencies and mode shapes of a given flexible structure. It is particularly well suited to the analysis of preliminary vehicle designs of the type under study here, as a full finite element model of the structure is not required.

The assumed modes method is based on Lagrange's equations, namely the set of n scalar equations

$$\frac{d}{dt}\left(\frac{\partial T}{\partial \dot{q}_i}\right) - \frac{\partial T}{\partial q_i} + \frac{\partial V}{\partial q_i} = f_i,\ i = 1, \ldots, n \tag{33}$$

where T is the total kinetic energy of the system, V is its potential energy, q_i its i^{th} generalized coordinate (e.g., displacement or rotation), and f its i^{th} generalized force (e.g., force or moment). The assumed modes method expresses the displacement along the structure as an expansion of the form

$$u(x,t) = \sum_{i=1}^{n} \psi_i(x) u_i(t) \tag{34}$$

where the shape functions $\{\psi_i(x),\ i = 1, \ldots, n\}$ are the assumed modes. These functions are termed admissible functions, meaning that they are linearly independent, satisfy all of the geometric boundary conditions of the structure, and possess all required derivatives.

The kinetic energy of the structure can then be written as

$$T = \frac{1}{2}\int_0^L \rho A \left(\frac{\partial u}{\partial t}\right)^2 dx \tag{35}$$

where $\rho A(x)$ denotes the mass per unit length of the structure. This can be re-written in matrix-vector form using the assumed modes expansion of Equation 34 as

$$T = \frac{1}{2}\dot{\boldsymbol{u}}^T M \dot{\boldsymbol{u}} \tag{36}$$

where $\boldsymbol{u} = \begin{bmatrix} u_1 & \cdots & u_n \end{bmatrix}^T$ and

$$M = \begin{bmatrix} m_{11} & \cdots & m_{1n} \\ \vdots & \ddots & \\ m_{n1} & & m_{nn} \end{bmatrix} \tag{37}$$

with

$$m_{ij} = \int_0^L \rho A \psi_i(x) \psi_j(x) dx \tag{38}$$

Dealing similarly with the potential (strain) energy of the structure,

$$V = \frac{1}{2} \int_0^L EI(x) \left(\frac{\partial^2 u}{\partial x^2} \right)^2 dx \tag{39}$$

gives the matrix-vector expression

$$V = \frac{1}{2} \boldsymbol{u}^T K \boldsymbol{u} \tag{40}$$

where

$$K = \begin{bmatrix} k_{11} & \cdots & k_{1n} \\ \vdots & \ddots & \\ k_{n1} & & k_{nn} \end{bmatrix}, \tag{41}$$

with

$$k_{ij} = \int_0^L EI \frac{\partial^2 \psi_i(x)}{\partial x^2} \frac{\partial^2 \psi_j(x)}{\partial x^2} \, dx \tag{42}$$

Note that $m_{ij} = m_{ji}$ and $k_{ij} = k_{ji}$ for all i and j, i.e., the matrices M and K are always symmetric.

The i^{th} generalized force, i.e., the i^{th} forcing term on the right-hand side of Equation 33, that arises from the pressure distribution p acting on an HSV together with point forces $\{u_j : j = 1, \ldots, m\}$ applied by control surfaces at positions $\{x_{sj} : j = 1, \ldots, m\}$ on the vehicle, can be written as

$$f_i(t) = \int_0^L p(x,t) \psi_i(x) \, dx + \sum_{j=1}^{m} u_j(x_{sj}, t) \psi_j(x_{sj}) \tag{43}$$

Forming the generalized force vector $\boldsymbol{f} = \begin{bmatrix} f_1 & \ldots & f_n \end{bmatrix}^T$, the n Lagrange's Equations (Equations 33) become finally

$$M \ddot{\boldsymbol{u}} + K \boldsymbol{u} = \boldsymbol{f} \tag{44}$$

The natural frequencies and mode shapes of the structure are obtained from the unforced harmonic dynamics of the system, i.e. setting $\boldsymbol{f} = \boldsymbol{0}$ and $\ddot{u} = -\omega^2 u$. The resulting eigenvalue problem is given by:

$$(\omega^2 I - M^{-1} K) \boldsymbol{u} = \boldsymbol{0} \tag{45}$$

The natural frequencies of the structure are thus the square roots of the eigenvalues of $M^{-1}K$; the corresponding mode shapes are given as linear combinations of the assumed modes, with the coefficients of these expansions given by the eigenvectors of $M^{-1}K$.

The assumed modes approach can be thought of as bridging the gap between, at the one extreme, the Rayleigh quotient method for estimating the fundamental natural frequency of a flexible structure and, at the other extreme, a full finite element analysis. The Rayleigh quotient method has the advantage of simplicity, but generally does not yield a very accurate frequency value; furthermore, it cannot be generalized to give estimates for the higher-order natural frequencies. The finite element technique, by contrast, is very general and powerful, but achieves this at the expense of simplicity. The assumed modes method, spanning these two limiting methods, allows the analyst to balance simplicity and accuracy of results as desired.

The connection between the assumed modes method and the Rayleigh quotient can be seen as follows. The Rayleigh quotient for a structure in bending, based on the expressions for the total kinetic and potential energy of the structure, can be written as

$$R(V) = \frac{\int_0^L EI\left(\frac{\partial^2 V(x)}{\partial x^2}\right)^2 dx}{\int_0^L \rho A V^2(x)\, dx} \tag{46}$$

where $V(x)$ is the assumed deflection function. It can be seen that this is identical to the eigenproblem produced by the assumed modes method for the case of a single assumed mode, $\psi_1(x) = V(x)$, i.e., the assumed modes method with $n = 1$ reduces to the Rayleigh quotient method. Note that, since the assumed deflection function in the Rayleigh quotient approach will include not only the desired fundamental true mode shape but also components of the higher-order modes, the resulting estimate for the fundamental natural frequency will always be an over-estimate for the true value. A similar observation also applies to the assumed modes method; however, increasing the number of assumed modes that are included, i.e. increasing the dimension n of the matrices M and K, will cause this estimate to decrease, improving convergence to the true value. Convergence to the lower true natural frequencies, i.e., those of most physical interest, is normally quite fast (assuming the assumed modes are chosen with some care), while the higher frequencies are slower to converge. By contrast, since the Rayleigh quotient is calculated using a single deflection function, no such freedom exists to control convergence.

The connections between the assumed modes method and the finite element method can be summarized as follows. The assumed modes method is more accurately described as the global assumed modes method, as the assumed mode shapes are defined over the entire structure. If instead the structure were to be broken up into small elements, with separate assumed modes defined to describe the deflections of each of these elements, and the elements then assembled to cover the entire structure, this approach would form the basis of the finite element method.

As noted previously, the shape functions $\{\psi_i(x),\, i = 1, \ldots, n\}$ that are used to set up the assumed modes method must be selected to be admissible functions, meaning that they are linearly independent, satisfy all of the geometric boundary conditions of the structure, and possess all required derivatives. A free-free structure such as the HSV has no geometric boundary conditions, so any set of linearly independent, sufficiently smooth functions actually can be used as an admissible basis. However, the convergence of the computed frequencies to the true natural frequencies of the structure will typically be faster if the assumed modes are selected with some care. In the present application, they are taken as the

mode shapes of a uniform free-free beam in bending, as this one-dimensional structure can be thought of as a very simplified model for the transverse vibrations of the flexible HSV. These mode shapes can be computed from the Bernoulli-Euler model (i.e. shear deformation and rotatory inertia neglected) of a uniform beam, with governing equation

$$EI\frac{\partial^4 u}{\partial x^4} + \rho A\frac{\partial^2 u}{\partial t^2} = 0 \tag{47}$$

where u denotes the transverse deflection. In order to solve for the natural frequencies and mode shapes of the beam, we assume simple harmonic motion, and can then write $u(x,t) = V(x)\cos(\omega t - \alpha)$: substituting this into Equation 47 yields the eigenvalue problem

$$EI\frac{d^4 V}{dx^4} - \omega^2 \rho A V = 0 \tag{48}$$

or

$$\frac{d^4 V}{dx^4} - \lambda^2 V = 0 \tag{49}$$

where $\lambda^2 = \omega^2 \rho A/(EI)$.

The general solution for this problem can be written in two forms:

$$V(x) = B_1 \sinh \lambda x + B_2 \cosh \lambda x + B_2 \sin \lambda x + B_4 \cos \lambda x \tag{50}$$

and

$$V(x) = C_1 e^{\lambda x} + C_2 e^{-\lambda x} + C_3 \sin \lambda x + C_4 \cos \lambda_x \tag{51}$$

Four unknowns must be determined in order to solve for the natural frequency and shape function (modulo scaling) corresponding to any given vibration mode: λ and essentially three of either $\{B_k : k = 1, \ldots, 4\}$ or $\{C_k : k = 1, \ldots, 4\}$. The two boundary conditions, either geometric or force-type, that exist at each end of the beam, give the four required constraints. For a free-free beam these conditions are that no shear force or moment can exist at the ends, giving

$$\left.\frac{\partial^2 V}{\partial x^2}\right|_{x=0,L} = 0 \tag{52}$$

and

$$\left.\frac{\partial^3 V}{\partial x^3}\right|_{x=0,L} = 0 \tag{53}$$

Although the expansions given by Equations 50 and 51 give, in principle, identical results, their behavior in practical computations can be very different. In fact, if Equation 50 is used to calculate the high-order mode shapes, severe rounding error problems will typically be encountered, to the point that the computed mode shapes bear essentially no resemblance to the actual free-free beam modes. The reason for this behavior arises from the expansions $\sinh \lambda x = (e^{\lambda x} - e^{-\lambda x})/2$ and $\cosh \lambda x = (e^{\lambda x} + e^{-\lambda x})/2$: for large λx, it can be noted that $\sinh \lambda x \approx \cosh \lambda x$ which is a large quantity. But it can be shown that the coefficients are approximately equal and opposite for the higher-order modes, so the expansion, Equation 50, involves subtracting two large, nearly equal quantities. Such near-cancellation is a classic way of introducing severe rounding errors in any computation carried out in finite-precision

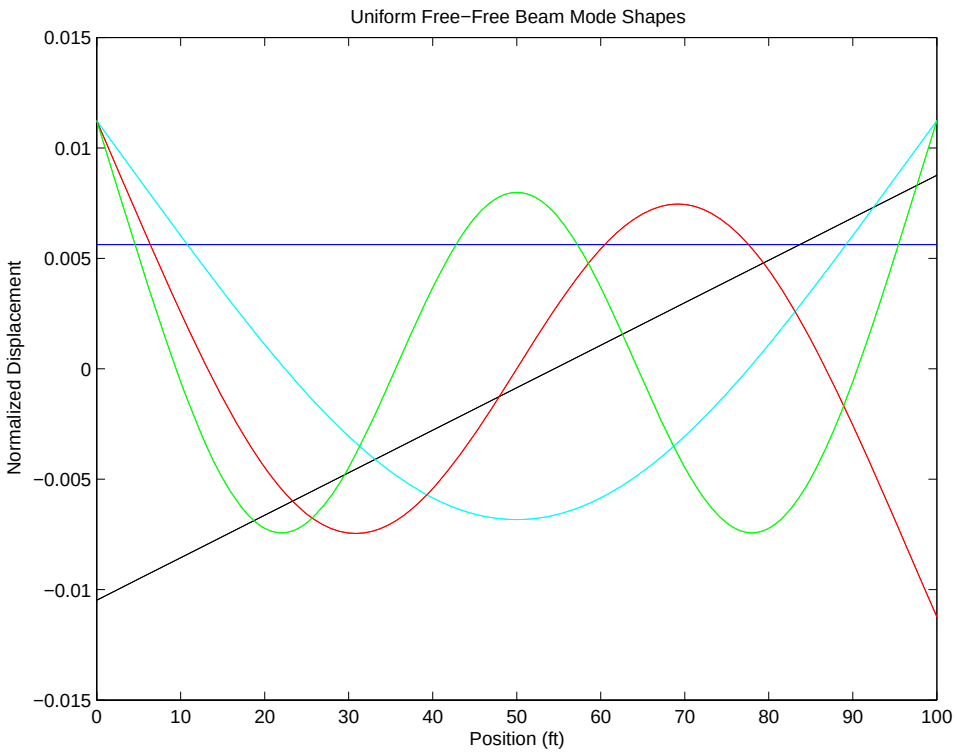

Figure 3. Modes Shapes for a Free-free Beam with Constant Properties

arithmetic, leading to the observed difficulties. If the expansion Equation 51 is used instead, such problems do not arise, giving the mode shapes plotted in Figure 3.

Another way of avoiding these numerical issues would be to make use of an alternative set of admissible functions as assumed modes. A set that is currently under study for the HSV problem is that of the *Chebyshev polynomials* $\{T_i(x) : i = 0, 1, \ldots\}$. These linearly independent functions (orthogonal in a certain sense) are defined over the range $x \in [-1, 1]$. Functions that are defined over any other desired range can be obtained by a linear transformation of the independent variable x. The Chebyshev polynomials possess certain desirable properties that render them useful in numerical analysis: notably, a given function of a real variable can be approximated by an expansion in terms of Chebyshev polynomials of prescribed degree more accurately than a truncated Taylor series of the same degree. In fact, it can be shown that the Chebyshev expansion of degree n for a given function $f(x)$ is a close approximation to the polynomial fit to $f(x)$ of degree n that minimizes the maximum error in the fit at any point.

Of more importance in the present application, the Chebyshev polynomials can be computed very simply by means of their defining three-term recursion

$$T_{i+1}(x) = 2xT_i(x) - T_{i-1}(x),\ i = 2, 3, \ldots \tag{54}$$

with this recursion initialized by $T_0(x) = 1$ and $T_1(x) = x$. (Note that, in structural terms,$T_0(x)$ can be thought of as a rigid-body translation mode and $T_1(x)$ a rigid-body rotation mode). Thus, for instance,$T_2(x) = 2x^2 - 1$, $T_3(x) = 4x^3 - 3x$, etc. However, there is no need to store any but the first two polynomials explicitly; it is more efficient to calculate them as needed using the three-term recursion. Note that the Chebyshev polynomials with

even indices are even functions of x, and those with odd indices are odd functions. Also, these dimensionless functions are bounded by values -1 and +1, as shown in Figure 4, and are, to a first approximation and modulo scaling, quite similar to the mode shapes of the uniform free-free beam, as can be seen by comparing Figures 3 and 4. The investigation of a Chebyshev polynomial-based assumed modes approach to the HSV problem is underway to determine whether there are any advantages to this approach.

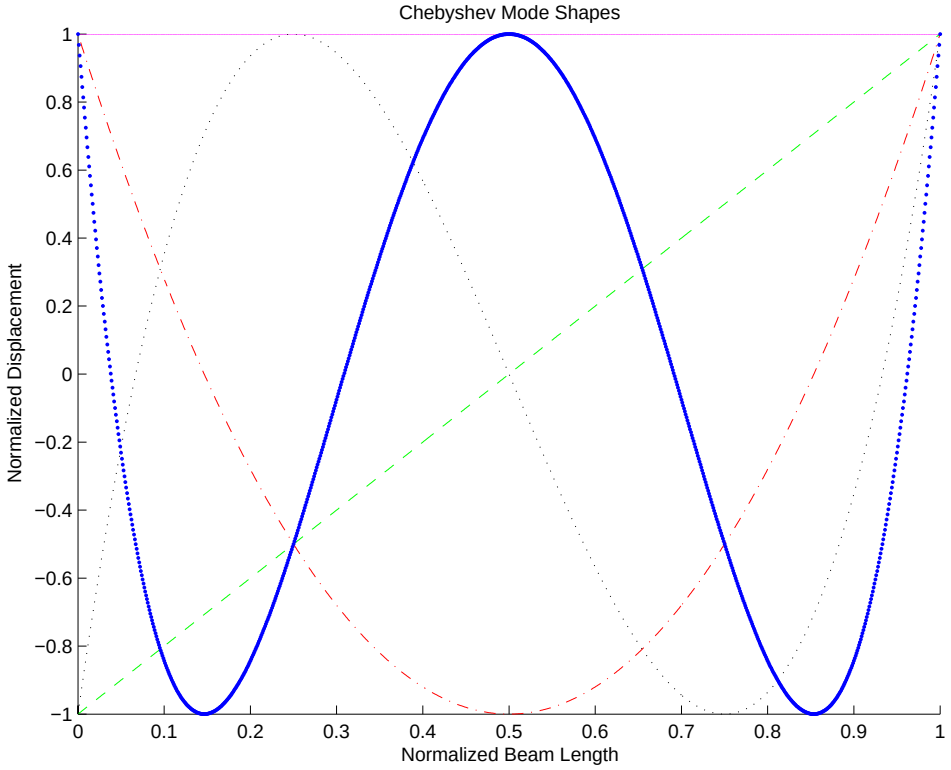

Figure 4. Chebyshev Polynomials, $\{T_i(x) : i = 1, \ldots, 5\}$

A key reason for carrying out the assumed modes analysis of the HSV was to determine how the structural dynamics of the vehicle change as propellant is consumed during the mission. Figures 5 through 6 provide this information by showing the first five flexible mode shapes for propellant quantities ranging from 100% to 0%; for clarity, propellant quantities corresponding to the initial rocket phase are shown in green, while those corresponding to the scramjet phase are shown in blue. It can be seen that, as a general rule, the deflection of the midsection of the vehicle increases as propellant quantity decreases,i.e., as the HSV tanks empty: since these tanks are grouped around the midsection, this observation makes sense. Note also that the slopes of the mode shapes at the positions of the control surfaces and of the proposed canard vary as a function of propellant quantity, leading to changes in closed-loop behavior during the course of the flight. The implications of this variation for closed-loop performance and robustness are currently under study.

Note that Figures 5 through 6 were computed using an assumed modes model containing six free-free beam flexible modes. To examine whether this number is adequate, Figure 7 demonstrates how the computed natural frequencies of the HSV converge to the true frequencies as the number of assumed modes is increased. Considering the fundamental frequency,

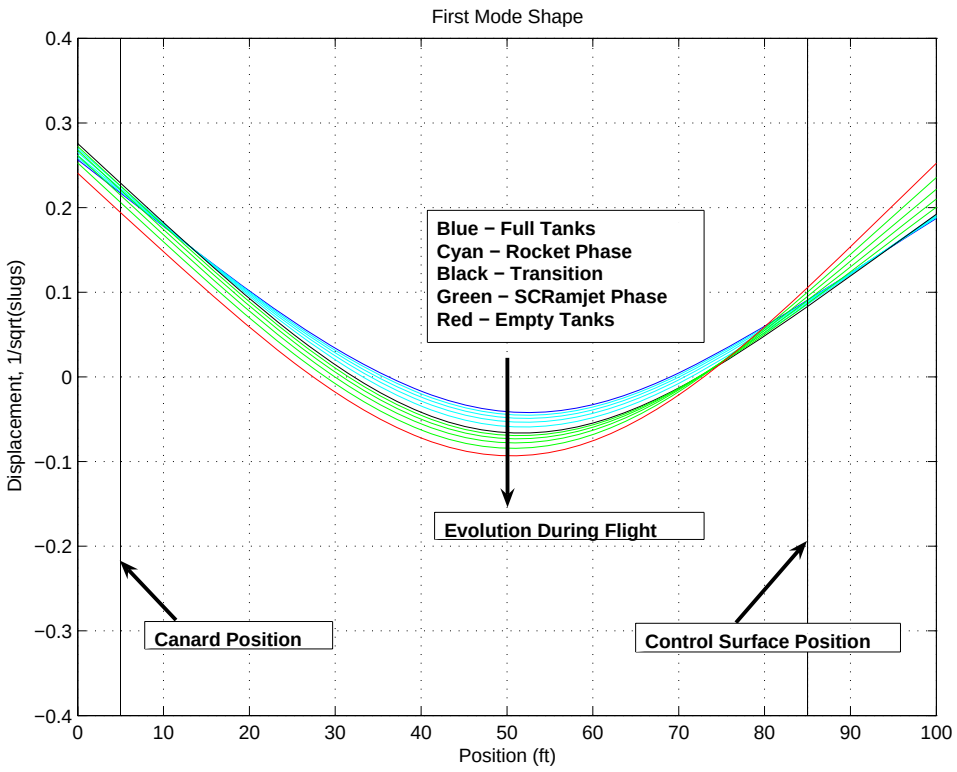

Figure 5. Evolution of First Mode Shape During Flight

it can be seen that using a single assumed mode gives a significant over-estimate for the true frequency (the method in this case reduces to the Rayleigh quotient); increasing the number of assumed modes causes the computed frequency to approach the true value quickly. At least two assumed modes are needed to produce an estimate for the second natural frequency, with an increased number of assumed modes leading to an improved estimate for this frequency; and so on. Figure 7 demonstrates the general rule that the estimates for the lowest natural frequencies, i.e., those of the greatest physical interest, are the first to converge under the assumed modes method.

Figure 8 shows the effect of propellant consumption on the natural frequencies of the first two flexible body modes of the HSV (again computed using a six assumed mode model): it can be seen that the frequencies increase as propellant is consumed, i.e., as the vehicle becomes lighter, which is expected. In addition, the HSV will also experience a significant increase in temperature as a result of aerodynamic heating as the mission progresses. This temperature increase will in turn lead to a noticeable decrease in the stiffness of its structural members, leading to another form of variation in its flexible body dynamics. Figure 8 provides a preliminary demonstration of this effect by plotting the natural frequencies that are obtained for an increase in HSV temperature from 70°F to 1500°F: the corresponding change in the Young's modulus of the structural members is based on the data presented in Vosteen[6] for RS-120 titanium alloy. In this preliminary analysis, the structural temperature was simply increased uniformly throughout the HSV: the result is a decrease in natural frequencies, but no change in the corresponding mode shapes. (In assumed modes terms, a uniform change in temperature corresponds to a uniform decrease in Young's modulus E, and

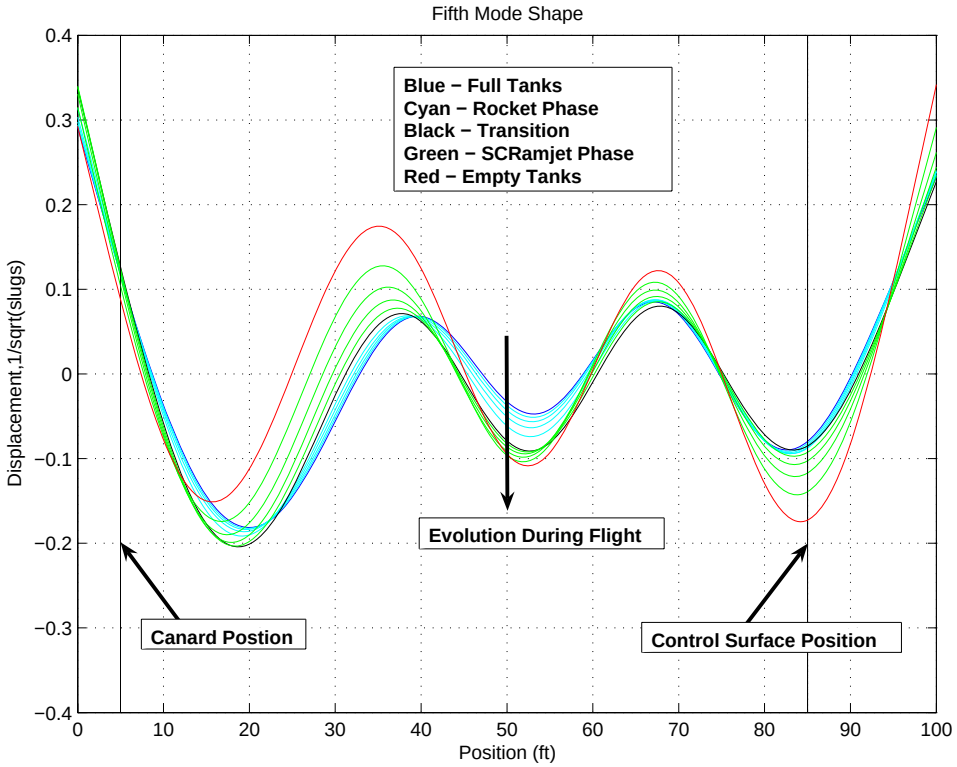

Figure 6. Evolution of Fifth Mode Shape During Flight

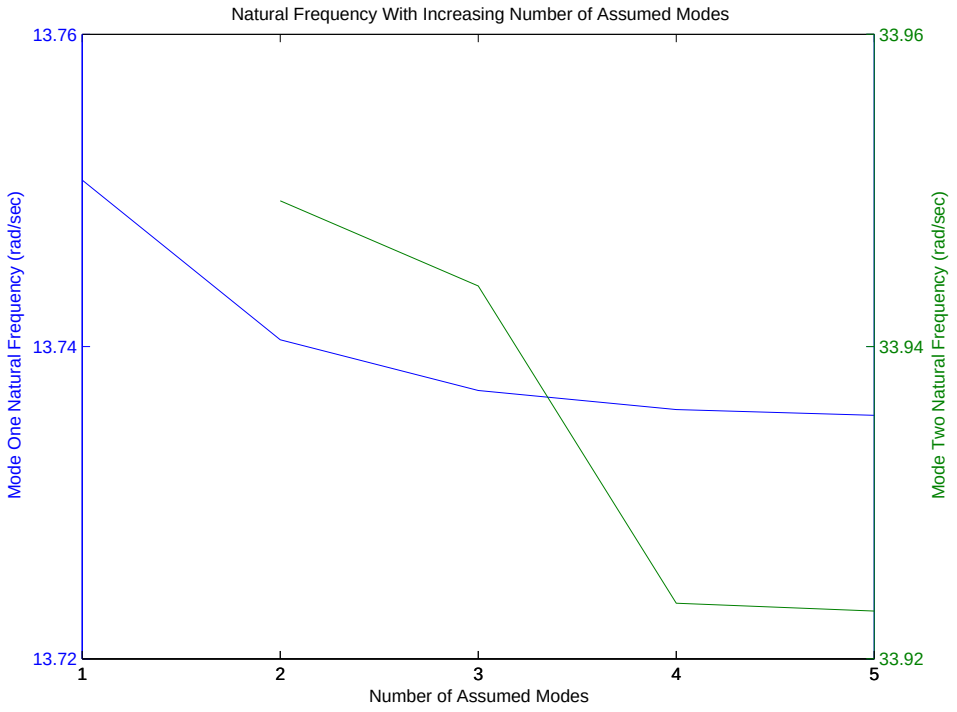

Figure 7. Convergence of Natural Frequency as Number of Assumed Modes is Increased

so to a simple scaling of the stiffness matrix K in Equation 40. This scales the eigenvalues (i.e., the natural frequencies) obtained from the eigenvalue problem Equation 45; however, the eigenvectors (mode shapes) are essentially unaffected.) A subject that is currently under investigation is an analysis of the actual variation in temperature not only along the vehicle, but also as a function of time throughout the mission. This improved analysis will yield not only natural frequencies, but also mode shapes, for the vehicle that take into account the evolution of both propellant mass and vehicle temperature distribution profile as the flight progresses. It is expected that such a model will provide more accurate estimates of the actual evolution of the HSV flexible body dynamics throughout its mission.

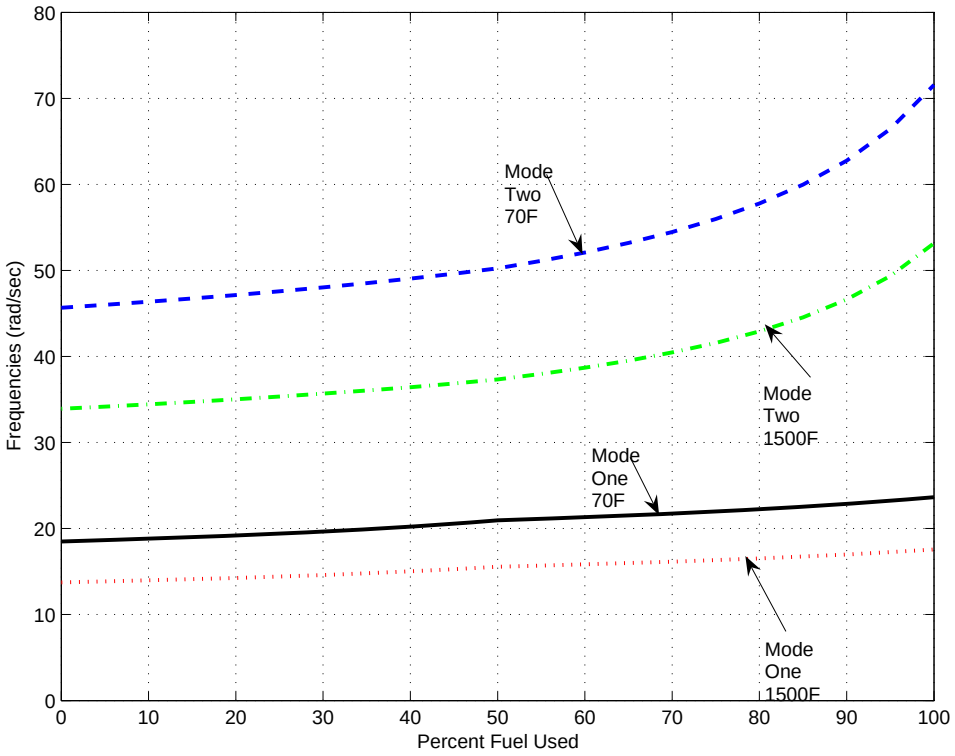

Figure 8. Effect of Mass on the Natural Frequencies

IV. Analysis of the Flight Dynamics

The analysis of flexible effects are important in the study of air-breathing hypersonic aircraft. The effect of the flexibility will cause changes to the overall flow field, thus altering the pressure distribution on the vehicle. For a hypersonic aircraft, the flexibility effects are exacerbated by the high level of coupling that is present in the system. Changes in the pressure distribution due to flexibility can be manifested as perturbations in thrust. As for all aircraft, the flexibility of the fuselage changes the angle-of-incidence for the control surfaces, thus affecting the control surfaces' ability to impart a desired control moment on the vehicle.

The longitudinal dynamics of a flexible aircraft, written in the stability axis coordinate

system are:[7]

$$\dot{V}_t = \frac{F_n \cos\alpha - D}{m} - g\sin(\theta - \alpha) \tag{55}$$

$$\dot{\alpha} = \frac{-L - F_n \sin\alpha}{mV_t} + Q + \frac{g}{V_t}\cos(\theta - \alpha) \tag{56}$$

$$\dot{Q} = \frac{M}{I_{yy}} \tag{57}$$

$$\dot{h} = V_t \sin(\theta - \alpha) \tag{58}$$

$$\ddot{\eta}_i = -2\zeta_i\omega_i\dot{\eta}_i - \omega_i^2\eta_i + N_i,\ i = 1, \ldots, n \tag{59}$$

where V_t is the true airspeed, F_n is the net thrust, D is the drag force, L is the lift, α is the angle-of-attack, θ is the pitch attitude, Q is the pitch rate, M is the pitching moment, I_{yy} is the moment-of-inertia, h is the altitude, ω_n is the structural natural frequency, ζ is the damping ratio, η_i is the modal coordinate for the i^{th} mode, and N_i is the generalized force corresponding to the i^{th} mode. In this case, the structural damping is given by $\zeta_i = 0.02$ and the structural dynamics are mass normalized. Any coupling between the rigid-body states and the elastic generalized coordinates occurs through the forces and moments. The forces and moments are dependent upon the pressure distribution, which is a function of the elastic deflection. In turn the deflection is a function of the generalized forces, N_i.

We will work with the equations-of-motion linearized about a reference constant altitude, constant Mach flight condition. We have assumed that $L_{\dot{\alpha}}$ and $M_{\dot{\alpha}}$ are negligible. We shall assume that three elastic modes are included in the aircraft model. The state vector is defined as

$$\boldsymbol{x} = \begin{bmatrix} \Delta V_T & \Delta\alpha & \Delta Q & \Delta h & \Delta\theta & \eta_1 & \dot{\eta}_1 & \ldots & \dot{\eta}_3 \end{bmatrix}^T \tag{60}$$

and the control vector is

$$\boldsymbol{u} = \begin{bmatrix} \Delta\delta_e & \Delta\delta_c & \Delta\delta_t \end{bmatrix}^T \tag{61}$$

The corresponding state matrix is given by

$$A = \begin{bmatrix} X_v & X_\alpha & 0 & X_h & -g & X_{\eta_1} & 0 & X_{\eta_2} & \cdots & 0 \\ \frac{Z_v}{V_{T_0}} & \frac{Z_\alpha}{V_{T_0}} & \frac{1-Z_q}{V_{T_0}} & \frac{Z_h}{V_{T_0}} & 0 & Z_{\eta_1} & 0 & Z_{\eta_2} & \cdots & 0 \\ M_v & M_\alpha & M_q & M_h & 0 & M_{\eta_1} & 0 & M_{\eta_2} & \cdots & 0 \\ 0 & -V_0 & 0 & 0 & V_0 & 0 & 0 & 0 & \ldots & 0 \\ 0 & 0 & 1 & 0 & 0 & 0 & 0 & 0 & \ldots & 0 \\ 0 & 0 & 0 & 0 & 0 & 1 & 0 & 0 & \ldots & 0 \\ N_{1,v} & N_{1,\alpha} & 0 & N_{1,h} & 0 & N_{1,\eta_1} & N_{1,\dot{\eta}_1} & N_{1,\eta_2} & \ldots & 0 \\ 0 & 0 & 0 & 0 & 0 & 0 & 0 & 0 & \ldots & 0 \\ N_{2,v} & N_{2,\alpha} & 0 & N_{2,h} & 0 & N_{2,\eta_1} & 0 & N_{2,\eta_2} & \ldots & 0 \\ 0 & 0 & 0 & 0 & 0 & 0 & 0 & 0 & \ldots & 1 \\ N_{3,v} & N_{3,\alpha} & 0 & N_{3,h} & 0 & N_{3,\eta_1} & 0 & \ldots & N_{3,\eta_3} & N_{3,\dot{\eta}_3} \end{bmatrix} \tag{62}$$

and the control influence matrix is

$$B = \begin{bmatrix} X_{\delta_e} & X_{\delta_c} & X_{\delta_t} \\ \frac{Z_{\delta_e}}{V_{T_0}} & \frac{Z_{\delta_c}}{V_{T_0}} & \frac{Z_{\delta_t}}{V_{T_0}} \\ M_{\delta_e} & M_{\delta_c} & M_{\delta_t} \\ 0 & 0 & 0 \\ 0 & 0 & 0 \\ N_{1,\delta_e} & N_{1,\delta_c} & N_{1,\delta_t} \\ 0 & 0 & 0 \\ N_{2,\delta_e} & N_{2,\delta_c} & N_{2,\delta_t} \\ 0 & 0 & 0 \\ N_{3,\delta_e} & N_{3,\delta_c} & N_{3,\delta_t} \end{bmatrix} \tag{63}$$

The definitions of the stability and control derivatives for a hypersonic vehicle are different from their textbook definitions (see Stevens and Lewis[8] for example) because there are functional dependencies that are present for hypersonic aircraft that can be neglected for subsonic aircraft. The main driver being that air-breathing hypersonic aircraft have an engine that is highly integrated into the airframe. Thrust is now dependent upon angle-of-attack, in addition to Mach Number and altitude. The lift and pitching moment are also functions of the thrust setting in addition to the states (e.g., Q and α) and the elevator. Therefore, these relationships must be captured in the stability and control derivatives. For example,

$$X_\alpha = \frac{1}{m}\left(\frac{\partial T}{\partial \alpha}\cos\alpha_0 - \frac{\partial D}{\partial \alpha} + L_0\right) \tag{64}$$

where the subscript $()_0$ denotes the trim value of a particular variable. The complete set linearized stability and control derivatives for a rigid hypersonic vehicle are found in Reference 9.

Our primary interest here will be on how the poles and zeros of the linearized system migrate as the vehicle mass changes. The issue of temperature effects on the structural frequencies and linearized aircraft dynamics are also addressed in Reference 10.

Given in Figure 9 is an example of how the poles and zeros migrate as a function of mass change for a cruise at Mach 8 and 85,000 ft. It was assumed that the temperature of the structure was a constant 100 °F. The transmission zeros in this case are for the input vector, $\boldsymbol{u} = [\delta_e\ \delta_t]^T$, and for the output vector $\boldsymbol{y} = [V_t\ \gamma]^T$. In each case that was analyzed, the short period dynamics are unstable, and the poles move away from the imaginary axis as the mass of the vehicle decreases. Note also as mass decreases, there is a corresponding decrease in the pitch moment-of-inertia. The short-period poles can be approximated by $s = Z_\alpha/(2V_t) \pm \sqrt{M_\alpha}$ for $M_\alpha > 0$ as in this case. Thus, one can see that the $1/m$ term in the Z_α derivative will become larger as m deceases. The same holds true for the $1/I_{yy}$ term in M_α. As seen in the section above, a reduction of mass corresponds to an increase in the natural frequencies of the mode shapes. For example, there is a 3 rad/s migration of the first flexible mode frequency from the beginning of the cruise to the end of the cruise. Upon closer investigation, the transmission zeros associated with the modal coordinates shift by the same amount as the poles as the mass of the vehicle is changed.

Note also that in Figure 9 that there are real, right-half plane transmission zeros, that have a near mirror image in the left-half plane. The presence of these right-half plane zeros

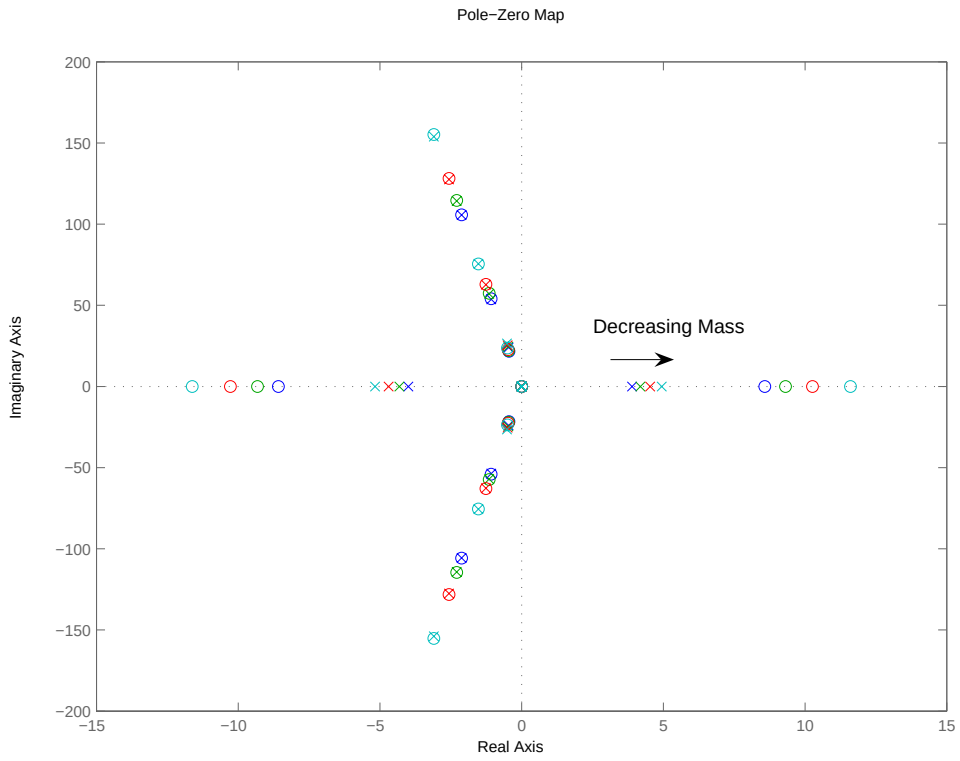

Figure 9. Pole-Zero Map for Cruise at Mach 8, 85000 ft

is due to the choice of elevator as the input and the flight path angle, γ as the output. To increase γ requires a trailing edge up deflection of the elevator. On an HSV, the elevators are large, and as such make a significant contribution to the total lift on the vehicle. When the elevator is deflected trailing edge up, the overall lift on the aircraft is decreased, causing an instantaneous drop in the center-of-gravity of the aircraft, which is characteristic of the non-minimum phase zero.

Because the aircraft is unstable and non-minimum phase, the control design problem becomes very difficult because the non-minimum phase zero imparts a real limit on the maximum achievable bandwidth of the control. Thus, it becomes necessary to change the configuration of the vehicle in order to mitigate the effects of the right-half plane zero. In Reference 9, the effects of adding a canard to both a rigid body HSV model and flexible HSV model are addressed. In the latter case, the structural model is more complex due to the assumptions made in constructing it, and as a result, there is significant inertial coupling between the rigid-body states and the flexible states. The analysis carried out in Reference 9 shows that there exists a static gain K, that in the case of the linearized rigid aircraft dynamics, that can be chosen to place the transmission zeros at an arbitrary location. The optimal location of the non-minimum phase zero is infinitely far to the right of the imaginary axis, thus giving the control designer infinite bandwidth. However, it was shown that the effects of flexibility on the transmission zeros will degrade the performance of the canard if it is ganged to the elevator by means of a static gain. What was thought to be an optimally placed non-minimum phase zero will now be brought closer to the imaginary axis, thus resulting in a limitation of the controller bandwidth.

Examining the effect of small perturbations in the Z_{δ_c} control derivative will result in what are not insignificant changes in the transmission zeros. In Figure 10 we show the nominal NMP transmission zero location at 11.2 rad/s for the input pair $\boldsymbol{u} = [\delta_e \, \delta_t]^T$ which is equivalent to no interconnect gain between the elevator and canard. We then calculate an interconnect gain by letting $Z_{\delta_e} + KZ_{\delta_c} = 0$. This places the NMP zero at 20 rad/sec. Next, we perturb the element in the control influence matrix that corresponds to Z_{δ_c} by $\pm 10\%$ and plot the migration of the system zeros. The NMP zeros change by as 20% due to 10 % increase in the Z_{δ_c}, while a 10% change results from a 10% decrease. This indicates that the changes in Z_{δ_c} that occur due to changes in the local angle-of-attack that are caused by the deflection of the fuselage will make the control design that much more challenging.

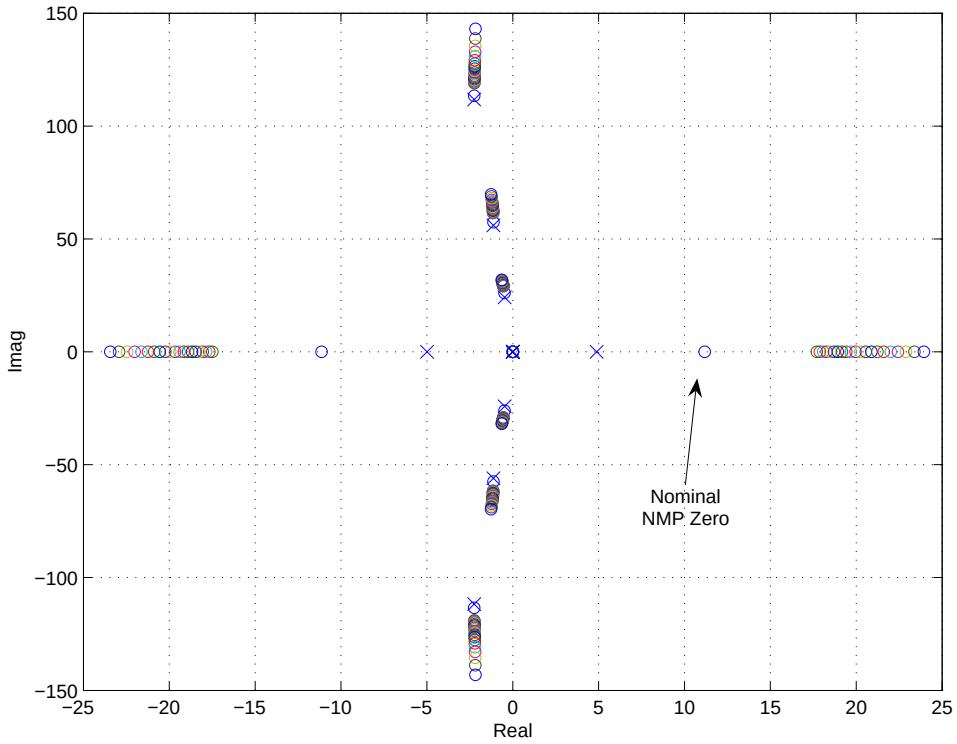

Figure 10. Changes in Transmission Zeros due to Perturbations in Z_{δ_c}

V. Conclusions

A method for estimating the structural dynamics of an air-breathing hypersonic aircraft has been given. The method that is outlined in known as the assumed modes method. A set of basis functions that satisfy the geometric boundary conditions are assumed to be known. Using the mass and stiffness distributions of the structure, the basis functions are used to form an eigenvalue problem that gives the estimated frequencies and mode shapes for the structure. As the number of assumed modes increases, the frequencies approach those of the actual structure.

The mode shapes for a generic HSV configuration were estimated. Included in the analysis were the effects of fuel consumption and temperature on the mode shapes and frequencies.

It was shown that mass has a significant influence on the natural frequencies, with the frequencies increasing as mass decreases. An effect on the mode shapes is seen, with some variance in the amplitude and the locations of the nodes. The effect of temperature on the structural dynamics was also modelled. The frequencies of the structure are dependent upon the Young's Modulus of the structure, which is a function of temperature. The effects of a uniform increase in temperature are to decrease the frequencies, but not affect the mode shapes.

Finally, the effects of mass change on the linearized vehicle were analyzed. The main concern was directed towards the short-period dynamics of the vehicle, which are open-loop unstable. The change in mass due to fuel burn moves the poles away from the imaginary axis as expected. In turn, the non-minimum phase zeros move farther away, but still impose a bandwidth restriction on the system due to their proximity to the right-half plane pole. The effects of a canard on the zero location were also studied. It was shown that for 10% variation in the lift due to canard control derivative, the non-minimum phase transmission zero can move by 20%. The movement of this zero closer to the unstable pole will have an adverse effect on the control system as the bandwidth will be reduced.

VI. Acknowledgement

The authors would like to acknowledge J. Carter for preparation of the figures for this paper.

References

[1]Bolender, M. and Doman, D., "A Non-Linear Model for the Longitudinal Dynamics of a Hypersonic Air-breathing Vehicle," *Proceedings of the 2005 AIAA Guidance, Navigation, and Control Conference [CD-ROM]*, Aug 2005, AIAA 2005-6255.

[2]Craig, R., *Structural Dynamics: An Introduction to Computer Methods*, Wiley, 1981.

[3]Czysz, P., Bruno, C., and Kato, K., "Interactions Between Propulsion Systems and the Configuration Concepts Defines the Design Space," 10^{th} *International Space Planes and Hypersonic Systems and Technologies Conference [CD-ROM]*, April 2001, AIAA 2001-1924.

[4]Gregory, T., Petersen, R., and Wyss, J., "Performance Tradeoffs and Research Problems for Hypersonic Transports," *Journal of Aircraft*, Vol. 2, No. 4, July-Aug. 1965, pp. 266–271.

[5]Czysz, P., *Hypersonic Convergence*, chap. 2, TBD.

[6]Vosteen, L. F., "Effect of Temperature on Dynamic Modulus of Elasticity of Some Structural Alloys," Tech. Rep. 4348, Langley Aeronautical Laboratory, Hampton, VA, August 1958.

[7]Waszak, M. and Schmidt, D., "Flight Dynamics of Aeroelastic Vehicles," *Journal of Aircraft*, Vol. 25, No. 6, June 1988, pp. 563–571.

[8]Stevens, B. A. and Lewis, F. L., *Aircraft Control and Simulation*, Wiley-Interscience, 1992.

[9]Bolender, M. and Doman, D., "Flight Path Angle Dynamics of Air-breathing Hypersonic Vehicles," AIAA 2006-6692.

[10]Bolender, M. and Doman, D., "Modeling Unsteady Heating Effects on the Structural Dynamics of a Hypersonic Vehicle," AIAA 2006-6646.